11-1-2023

Topological optimization of flow-shifting microchannel heat sink

S. Ozguc

L. Pan

Justin A. Weibel
jaweibel@purdue.edu

Ozguc, S.; Pan, L.; and Weibel, Justin A., "Topological optimization of flow-shifting microchannel heat sink" (2023). *CTRC Research Publications.* Paper 404.
http://dx.doi.org/https://doi.org/10.1016/j.ijheatmasstransfer.2023.123933

International Journal of Heat and Mass Transfer 207 (2023) 123933

Contents lists available at ScienceDirect

International Journal of Heat and Mass Transfer

journal homepage: www.elsevier.com/locate/hmt

Topological optimization of flow-shifting microchannel heat sinks

Serdar Ozguc, Liang Pan, Justin A. Weibel*

Cooling Technologies Research Center and School of Mechanical Engineering, Purdue University, 585 Purdue Mall, West Lafayette IN 47907, United States

ARTICLE INFO

Article history:
Received 2 December 2022
Revised 23 January 2023
Accepted 2 February 2023

Keywords:
Electronics cooling
Microchannel
Heat sink
Topology optimization
Multi-objective optimization

ABSTRACT

Efficient thermal management is required for electronic devices that generate multiple different spatially nonuniform thermal workloads during operation. Conventional heat sinks route coolant to all potential heat-generating regions of an electronic component which may result in unnecessarily broad dispersion of the coolant to regions that are sometimes inactive. To fully utilize flow for multiple potential thermal workloads, a "flow-shifting" design approach is proposed. A flow-shifting heat sink has multiple inlets, where the flow path from each inlet is optimized for cooling of a specific workload or heat map. Only the inlet corresponding to the active operating workload is open at a given time, while the rest of the inlets are kept closed until the operating workload changes, allowing a majority of the flow to be properly utilized for cooling the active heat map. This has the potential to allow many different optimal heat sinks to be simultaneously encoded into a single structure but brings forth a complex design problem to optimize the internal fluid flow pathways. A multi-objective topology optimization algorithm is implemented in this work for flow-shifting heat sink design generation. Microchannel heat sink designs are generated for a demonstration case involving two workloads. Designs optimized for flow-shifting between two inlets are compared to a benchmark that is optimized with only a single inlet. Pareto optimality curves, as well as the associated heat sink designs, are created that weigh between the thermal resistances of the two workloads. The flow-shifting designs are predicted to have lower thermal resistance under both workloads compared with every benchmark heat sink design generated along the Pareto optimality curve. Investigation of two designs selected from the Pareto curve showed that the flow-shifting heat sink achieved 10.7% and 6.8% lower thermal resistance at the two workloads relative to the benchmark. The flow-shifting approach is superior as it utilizes more flow rate for cooling the active heated region. The flow-shifting approach thereby allows for fixed heat sink structures that can be topologically optimized for many different possible heat maps and actively respond to changes in workload.

Introduction

Continuous downscaling of electronic device size needs efficient heat removal from increasingly compact spaces, which drives the development of thermal management technologies for higher performance. Air- and liquid-cooled heat sinks are widely used with optimized shapes to effectively reject heat. Topology optimization has been applied to improve the performance of heat sinks under the various boundary conditions engendered by different applications. Topology optimization is a mathematical design algorithm that optimizes material distribution within the design space for a user-defined objective function and has been implemented in many different engineering applications due to its ability to generate designs that would be difficult or impossible to devise using conventional design approaches.

This method has been implemented in various ad hoc electronics cooling applications and the heat sink designs have been shown to improve performance relative to conventional benchmark designs. Zeng et al. [1] developed a two-layer 2D numerical model and used topology optimization to generate heat sink designs for air-cooling applications. The designs were fabricated using conventional machining techniques and experimentally characterized, achieving a 55% lower pumping power while maintaining the same thermal performance as a conventional straight-channel heat sink. Koga et al. [2] adopted a Stokes flow model assumption and performed topology optimization of liquid-cooled heat sinks to minimize pressure drop and maximize heat dissipation. Dede [3] used topology optimization to generate a multipass branching microchannel heat sink (MCHS) which consisted of two separate topology optimized layers and leveraged characteristics of both jet impingement and microchannels. Zhou et al. [4] topologically optimized the microchannels within a manifold MCHS design which showed decreased pressure drop and thermal resistance compared to a manifold microchannel heat sink with straight microchan-

* Corresponding author.
E-mail address: jaweibel@purdue.edu (J.A. Weibel).

https://doi.org/10.1016/j.ijheatmasstransfer.2023.123933
0017-9310/

Nomenclature

A	design domain footprint area, m^2
c_p	coolant specific heat capacity, J/kg-K
f_{cost}	cost function
H	fin/channel height, m
H_b	base thickness, m
k_f	coolant thermal conductivity, W/m-K
P_{in}	inlet static pressure, Pa
Q	heat input, W
R	thermal resistance, K/W
R_p	pseudo thermal resistance, K/W
T_b	base temperature, K
t_f	fin thickness, m
T_{in}	inlet coolant temperature, K
T_{max}	maximum base temperature, K
u_{in}	inlet flow speed, m/s
w_c	channel width, m
Δx	grid cell size, m

Greek Symbols

α	weighting coefficient, -
ε	design variable, -
μ	dynamic viscosity, Pa-s
ρ	density, kg/m^3

Acronyms

AM	additive manufacturing
DMLS	direct metal laser sintering
HI	heterogeneous integration
MCHS	microchannel heat sink
TO	topology optimization

nels/fins of optimized width. Dilgen et al. [5] performed a fully 3D topology optimization of liquid cooled heat sinks with turbulent flow. Joo et al. [6] topologically optimized heat sinks in natural convection with a proposed surrogate model that accounted for the shape-dependent variation of the heat transfer coefficient. Their topologically optimized heat sink was predicted to have 15% lower thermal resistance and 26% less mass compared to their benchmark design. Martinez-Maradiaga et al. [7] used topology optimization to generate a natural convection heat sink for thermal management of a commercial tablet. This past work has shown that topology optimization brings significant performance benefits for thermal management applications, however, the resulting designs are often complex in shape. On the other hand, recent advancements and commercialization of metal additive manufacturing (AM) technologies provided design freedom that makes it a suitable method for the fabrication of complex geometries generated by topology optimization. For example, Dede et al. [8] generated an air-cooled heat sink design using topology optimization, fabricated the design with additive layer manufacturing in AlSi12, and their experimental results showed a higher coefficient of performance compared to the conventional benchmark designs. Lazarov et al. [9] generated a passively cooled heat sink using topology optimization for LED cooling, 3D printed the design, and experimental tests showed a 21% decrease in temperature relative to the benchmark industry solutions.

Most previous work on topology optimization of heat sinks has focused on heat sources which are uniform in space and constant in time. However, such conditions are not representative of real applications; there is an interest in thermal management devices for non-uniform heating [10,11] and time-dependent workloads [12,13,14]. Few topology optimization studies have considered either non-uniform or time-dependent heating. Li et al. [15] performed topology optimization of liquid-cooled heat sinks, but investigated designs generated for cooling of spatially nonuniform heat sources, with an experimental demonstration of an 11.7% lower maximum surface temperature compared to a conventional straight channel design. Dong and Liu [16] used multi-objective topology optimization to generate air-cooled heat sink designs for a thermal problem involving three separate heaters. These studies looked into non-uniform heating; however, the heat maps were constant in time. On the other hand, Iradukunda et al. [17] performed topology optimization for a phase change material integrated heat sink for applications involving fast transients. They fabricated their design using DMLS in AlSi10Mg and experimentally showed an 18.9 °C decrease in peak temperature relative to a plate fin heat sink design at a pulsed load of 50 W. Banthiya et al. [18] investigated the transient response of topology optimized air-cooled heat sinks. They showed that intuition-based design changes are needed alongside a steady state topology optimization when solving a non-steady thermal problem. These studies have looked into the transient effects of a single workload with varying power or switching between on and off states.

The next-generation electronics involve multiple components embedded within a single chip, referred to as heterogeneous integration (HI), and are often multi-functional. That is, they are expected to carry out different sets of operations at different times which result in multiple different non-uniform thermal workloads. Cooling solutions designed for a single heat map will not perform well when the workload is changed, because of a subsequent change in the thermal boundary condition. Ideally, several different heat sinks can be designed for the possible workloads, however, this is not a practical solution because it would require the heat sinks to be physically changed during operation in response to a change in the thermal workload. This work introduces a new "flow-shifting" heat sink design approach for liquid-cooling applications to address the thermal management challenges brought by electronic devices that often operate with different workloads (and thereby at heat maps) at different times of operation.

A schematic description that illustrates the concept of a flow-shifting heat sink designed for three different workloads is shown in Fig. 1, with a comparison to a conventional heat sink having only a single inlet to cool all heat loads. A flow-shifting heat sinks approach uses multiple inlet ports, with each inlet dedicated to a different device workload, in contrast with most heat sinks that have a single inlet port used for all operating conditions. Each inlet port is opened only when its assigned workload operates and is otherwise closed. The flow-shifting heat sink structure between the inlets and outlet must then be a single flow structure that is optimized simultaneously for all of the different hydrodynamic and thermal boundary conditions resulting from having multiple sets of inlet ports and workloads. When the workload changes, this same physical structure can be used to get a different effective heat sink response by changing the open inlet port and therefore shifting the flow to a more optimal path designed for the current workload. The result is a single part that is encoded with many different heat sinks that are optimal for multiple workloads, where in the ideal case, each encoded heat sink is as good as if a unique part were designed for a specific workload.

Although the flow-shifting heat sink concept is independent of the design algorithm used, it presents a complex design problem where intuition-based design is not likely to yield the desired ideal functionality and performance. Topology optimization is an enabling method that can unlock this functionality due to its ability to address the multi-objective nature of the design problem. Similarly, the approach is independent of the method of fabrication, however, metal AM technologies complement the pro-

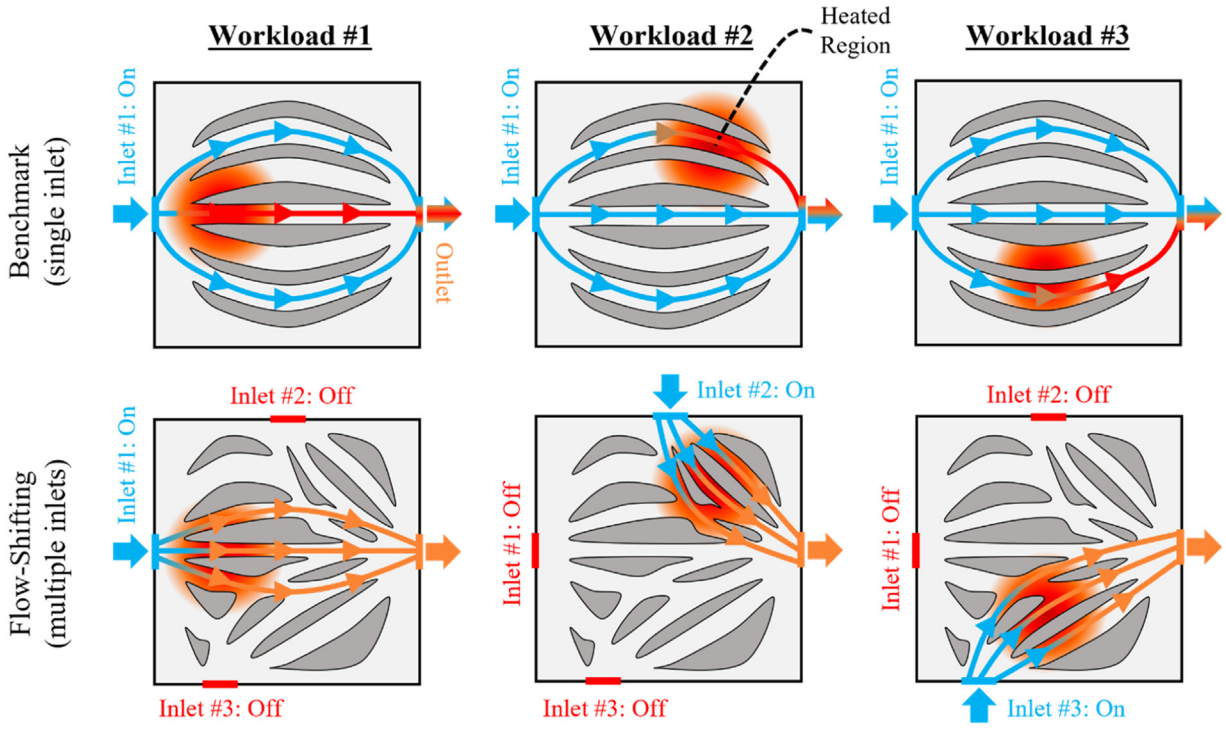

Fig. 1. Schematic top-down drawings of two heat sinks attached to a device operating at one of the three different workloads at a given time. A benchmark approach (top) uses a single inlet for all the workloads which leads to non-optimal flow paths where a portion of the coolant is not utilized effectively. The flow-shifting approach (bottom) uses three inlets. Each inlet is only opened when its dedicated workload is active. Flow paths are designed for specific workloads through optimizing heat sink geometry, and therefore the coolant is fully utilized.

posed approach due to their capability to fabricate the resulting topologically optimized designs that would be difficult to manufacture using conventional methods. In our previous work [19], we have formulated a homogenization approach where the partial densities are physically represented as porous microstructures during topology optimization. This formulation reduced the computational costs associated with topology optimization by allowing designs with sub-grid features. The homogenization approach has been shown to be a promising algorithm for designing microchannel heat sinks for complex boundary conditions and therefore is implemented in this paper to demonstrate the flow-shifting heat sink concept.

In summary, this work introduces the flow-shifting heat sink design approach to address the thermal challenges of next-generation electronics which involve multiple non-uniform workloads that change with time. The flow-shifting approach leverages multiple inlet ports each dedicated to a single workload and a single heat sink geometry optimized for the resulting complex boundary conditions. The result is a single heat sink structure that can address multiple different workloads as if it was optimized for each. The contents of this paper are as follows: the design spaces and workloads used in the case study are defined; the flow-shifting approach and the benchmark approach are explained; the topology optimization algorithm is briefly summarized; the multi-objective optimization problem is formulated; and the resulting designs and performance for the case study are discussed.

Methodology

Design case

The proposed flow-shifting approach is evaluated by comparing it with a benchmark approach using a single inlet. Heat sink designs are generated using both the flow-shifting and single-inlet approaches for a case study having two different workloads in the 30 mm × 30 mm design space as illustrated in Fig. 2. The design cases only differ in their inlet boundary locations to account for the multiple inlets needed by the flow-shifting approach. The two heated regions are marked as workload #1 and workload #2, where each workload would operate individually at different times and heat is applied uniformly over the shaded region. While this case is kept simple for demonstration purposes, any number of highly nonuniform heat maps could be posed to represent heterogenous electronic device workloads. Unheated header regions are added near the inlets and the outlet to give the flexibility to the optimization algorithm to route coolant before entering the heated regions. The benchmark approach uses the same single inlet irrespective of the operating workload. The flow-shifting approach assigns inlet #1 and inlet #2 to workload #1 and workload #2, respectively. The inlets are sized so that the flow enters the design space from a single inlet of the same size and with the same hydrodynamic boundary condition for both approaches, but the positions of the two different inlets must be offset for the flow-shifting approach.

The outlet is set to a constant reference pressure and a total inlet pressure boundary condition is applied with a value of 1.0 kPa (gage pressure relative to the outlet). The total pressure is defined as follows.

$$P_{tot} = P_{in} + \frac{1}{2}\rho u_{in}^2 \tag{1}$$

where P_{in} is the static pressure and u_{in} is the flow velocity at the inlet. A specified constant total pressure at the inlet is equivalent to a pump curve boundary condition, where a higher pressure drop from the inlet to outlet will result in a lower flow rate. This ensures that the heat sink designs need to have a low flow resistance to sustain adequate coolant flow. Each workload receives

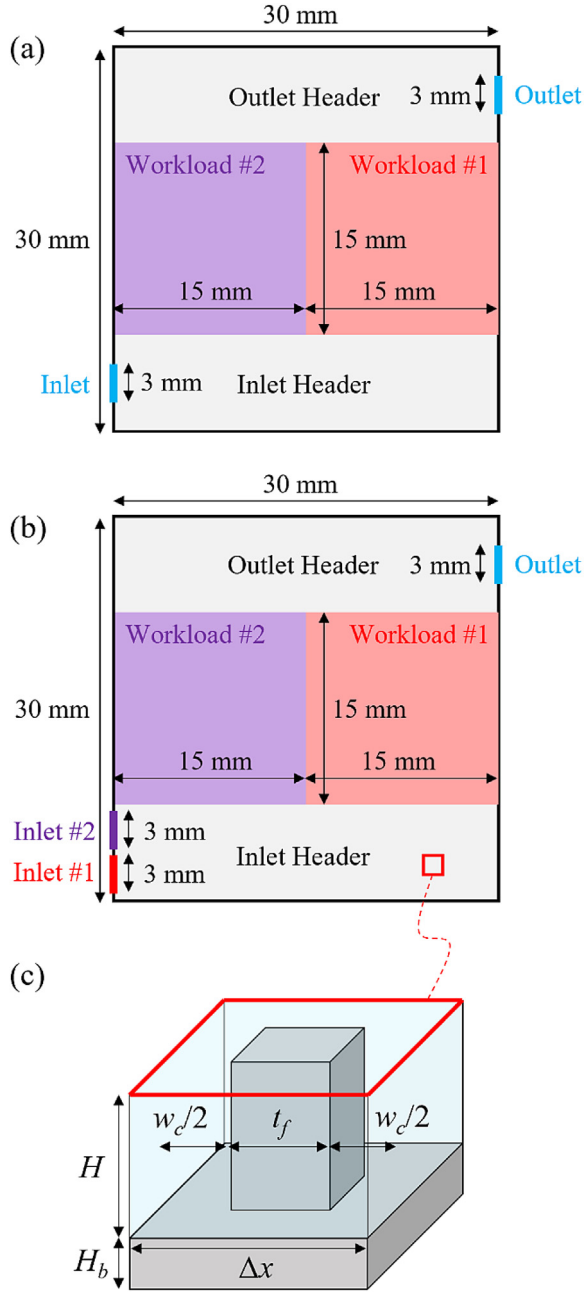

Fig. 2. Schematic top-down drawings of the design spaces and boundary conditions used for the (a) benchmark single-inlet and (b) flow-shifting approaches. There are a total of two workloads which can be active at a given time, but not simultaneously. The design spaces are discretized into (c) small square cells each with a square pin fin with the labeled dimensions. Some dimensions are omitted for legibility; however, features are drawn to scale with respect to the overall design space.

Table 1
Properties of water evaluated at 30 °C [20].

ρ (kg/m^3)	μ (Pa•s)	c_p (kJ/kg)	k_f (W/(m•K))
995.8	803.4•10^{-6}	4.178	0.6172

100 W applied uniformly over their 15 mm × 15 mm areas during operation. The coolant is water, assumed incompressible with temperature-independent thermophysical properties taken at 30 °C (Table 1).

Topology optimization

Heat sink designs are generated for both the benchmark single-inlet and the flow-shifting approaches using the homogenization approach to topology optimization developed by Ozguc et al. [19] in our previous work. The design spaces shown in Fig. 2 are discretized into small square grid cells with edge length Δx; each cell is assigned a design variable ε_i which represents the dimensions of a single square pin fin centered within the cell. Fig. 2.c shows a schematic drawing of a pin fin within the grid cell with the dimensions labeled. The design variable is defined as follows.

$$\varepsilon_i = \frac{\Delta x - t_{f,i}}{\Delta x} = \frac{w_{c,i}}{\Delta x} \tag{2}$$

where $t_{f,i}$ is the thickness of the fin and $w_{c,i}$ is the remaining channel width along the center cross-section of the grid cell. The design variables of each grid cell can be within the range 0 to 1 and therefore the fin thicknesses can vary within the range 0 to Δx. A gradient-based optimization algorithm is used to simultaneously optimize all the design variables to minimize a user-defined cost function which results in a topology optimized design. Per the grid discretization and design variable definition, the algorithm is given freedom to generate heat sink designs that vary in 2 dimensions; however, the heat sinks are modeled during optimization considering the 3-dimensional geometric features. There are two separate layers along the height. The coolant flows through the top design layer which consists of the optimized fins and channels. The bottom layer is a completely solid base to which the heat is applied. The bottom layer (H_b) and the top layer (H) are each 1 mm in height, resulting in a total heat sink thickness of 2 mm. The heat sink solid material is assigned a thermal conductivity of 160 W/m-K corresponding to an aluminum alloy (AlSi10Mg) commonly used for direct metal laser sintering [21].

In this study, the topology optimization approach implemented has been described in our previous work [19]. A brief description of the overall TO process is summarized here but readers are referred to Ozguc et al. [19] for a more detailed description. Topology optimization generally consists of an iterative sequence of physical models and optimization algorithms. Each TO run starts by initializing all the design variables within a design space with some initial value of ε_0. Then the optimizer enters into a loop where the performance of the design is iteratively improved by adjusting the design variables to minimize a cost function (i.e., the design objective). First, the design variables are filtered using the density filtering scheme of Sigmund et al. [22] to avoid the checkerboard problem commonly seen in topology optimization. In this work, a filter radius of 3 mm is used for the first 50 iterations, which is then reduced to 0.75 mm until convergence. After filtering, the velocity, pressure, and temperature profiles of the current design are calculated by numerically solving the governing partial differential equations described in detail previously in Ozguc et al. [19].

As a brief summary, these governing equations consist of 2D mass, momentum, and energy conservation equations for the top layer of the MCHS which encompasses the coolant flow through the pin fins. Viscous shear stresses and heat transfer from the pin fin surfaces are captured by using a porous media approach wherein effective permeability and heat transfer coefficient correlations for fully developed flow in pin fins are implemented. Another 2D energy conservation equation is used to model the heat transfer within the bottom layer which consists of the completely solid base. The energy equations are coupled together using source terms with effective interfacial heat transfer coefficients which are derived using height averaging operations. This low-computation-cost approach models laminar fluid flow and heat transfer in the heat sink using 2D conservation equations, but still accounts for important 3D effects such as the heat spreading in the

base layer and the velocity/temperature gradients along the height of the channels/fins using source terms. The 2.5D partial differential equations derived by the conservation laws are discretized using the finite volume method and solved using the software package Ansys Fluent.

Unique to the implementation for the flow-shifting approach in this work, because there are two workloads, the model solves for two sets of velocity, pressure, and temperature profiles for a given design corresponding to these different boundary conditions. The adjoint state method is used to perform a sensitivity analysis where the gradients of the cost function with respect to each of the design variables are calculated. Lastly, a sequential linear programming algorithm is used to update the design variables based on the calculated gradients. A convergence criterion of 200 fixed iterations is used for this work, which is found to be more than adequate for all of the designs to converge (i.e., no further change in the design or objective function with additional iterations). The choice of the grid cell size has been shown to affect the resulting designs for the homogenization approach [19], and must be sufficiently small to achieve near-optimal performance. This study uses a value of $\Delta x = 0.5$ mm because further refinement of the grid size was found to result in an insignificant change in performance.

Cost function

Topology optimization minimizes a user-defined cost function that is a mathematical representation of the design objectives. For microchannel heat sinks with a prescribed total inlet pressure, the design objective is to minimize a thermal resistance R defined as follows.

$$R = \frac{T_{max} - T_{in}}{Q} \tag{3}$$

where T_{max} is the resulting maximum heat sink temperature, T_{in} is the inlet temperature of the coolant, and Q is the heat input. However, the location of the maximum temperature within the design space can change during optimization which creates an ill-conditioned optimization problem. Therefore, an optimizer-friendly pseudo thermal resistance R_p is formulated as follows.

$$R_p = \frac{1}{Q}\left[\frac{1}{A}\int_A (T_b - T_{in})^m dA\right]^{\frac{1}{m}} \tag{4}$$

where A is the design space area and T_b is the spatially varying heat sink base temperature. With this formulation, the thermal resistance is affected by all temperatures in the heat sink base throughout the design, but placing more emphasis on higher temperatures compared to standard averaging. A higher value of the user-defined parameter m places more emphasis on higher temperatures. A value of $m = 4$ is found to result in designs having low maximum temperatures without converging issues and is used throughout this study.

During optimization, two different thermal resistance values are calculated for a heat sink operating at each of the two workloads. The optimizer needs to create designs that minimize the thermal resistance across both operating conditions. Therefore, a multi-objective cost function is formulated as the weighted summation of the thermal resistances of each workload.

$$f_{cost} = \alpha \cdot R_{p,1} + (1 - \alpha) \cdot R_{p,2} \tag{5}$$

where $R_{p,1}$ and $R_{p,2}$ are the pseudo thermal resistances of a given design at each respective workload #1 and #2, and α is the weighting coefficient. The weighting coefficient is a user-defined parameter within 0 – 1 and represents the importance given to $R_{p,1}$ over $R_{p,2}$ by the optimizer. A set of Pareto optimal designs is created by generating topology optimized designs with different weighting coefficients. These Pareto optimality curves can then be compared between the single-inlet benchmark and the flow-shifting approaches.

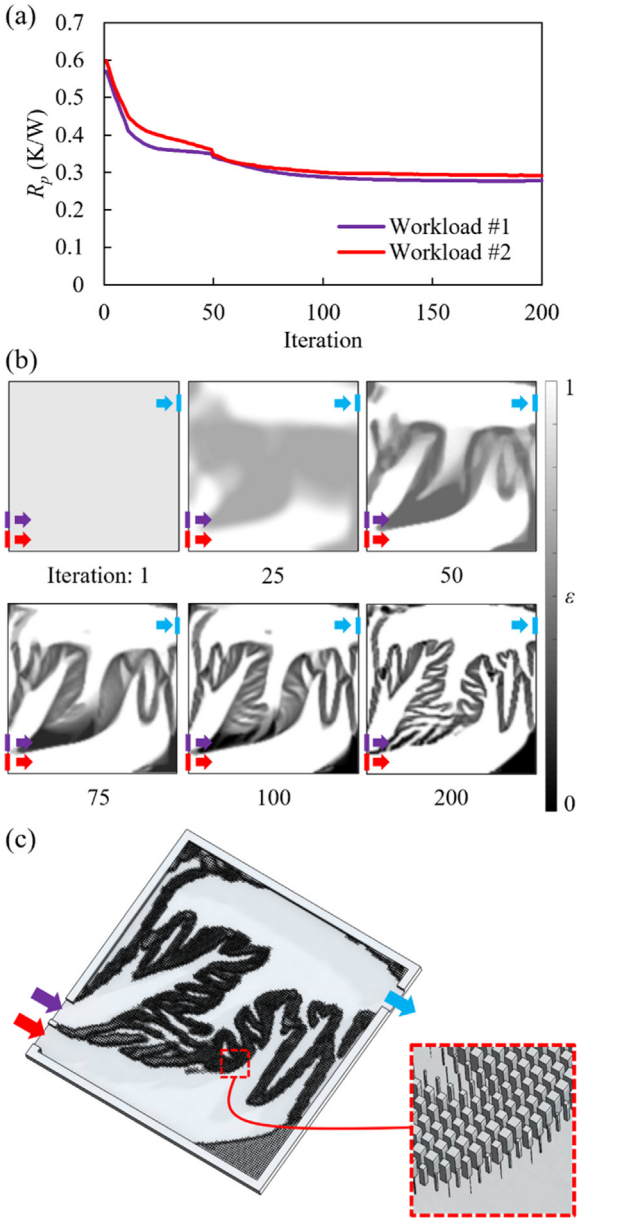

Fig. 3. (a) Pseudo thermal resistances of a flow-shifting heat sink design throughout optimization process, (b) design variable distribution maps at several iterations, and (c) CAD drawing of the final design and a close-up image of the pin fins.

Results

As described in the Methodology section above, topology optimization is an iterative algorithm where an initial design is updated at each iteration to minimize the multi-objective cost function f_{cost} (Eq. (5)). The results shown in Fig. 3.a and b summarize how the heat sink design and the corresponding thermal resistances change throughout the optimization process for an example case ($\alpha = 0.5$, $\varepsilon_0 = 0.9$) using the flow-shifting approach. Fig. 3.a shows the evolution of the pseudo thermal resistances associated with each workload as the iterations proceed; the contour plots above show the design variable distribution throughout the design space at several selected iterations. The thermal resistances continuously decrease until they converge to approximately con-

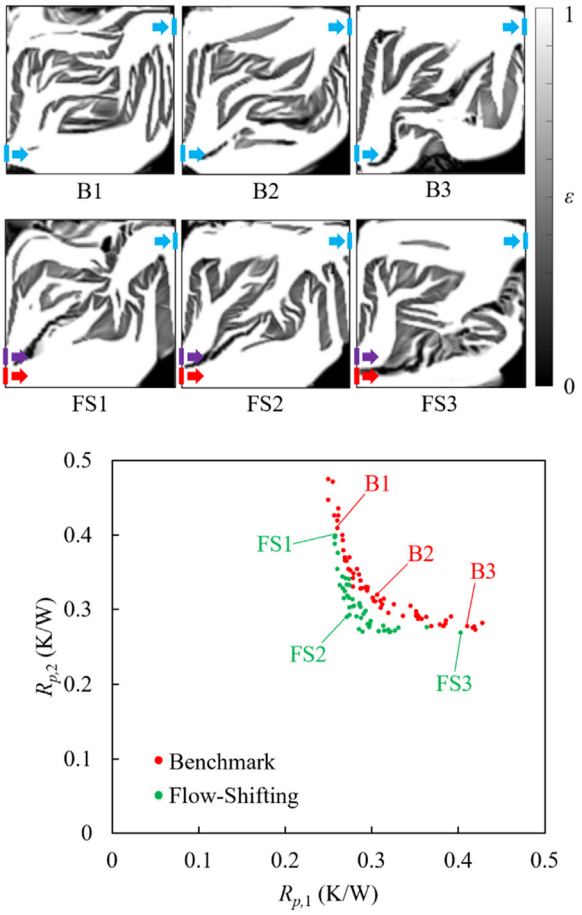

Fig. 4. Pareto optimality curves for the benchmark and the flow-shifting approaches. Each design is generated by seeding the optimizer with a random initialization and a random weighting coefficient. Three designs from each curve are shown above with the inlet and outlet ports labeled.

stant values after the 150th iteration. There is an abrupt change in the thermal resistances around the 50th iteration, which corresponds to the user-defined change in filtering radius from 3 mm to 0.75 mm, allowing the optimizer to create finer features within the design space. The grayscale contour maps in Fig. 3.b show the design variable distribution throughout the design space for several different selected iterations, where dark gray regions represent thick pin fins with tight spacing, lighter gray regions represent thinner pin fins with larger spacing, and white regions represent the open flow channels without pin fins. A 3D CAD drawing of the final design at the 200th iteration is shown in Fig. 3.c. The design consists of large open flow regions connected to each inlet and the outlet. The open flow regions are separated from each other by boundaries of tightly packed arrays of pin fins. There is a distinct pin fin boundary between the two inlets to ensure the flow from the inlets is routed to the heated regions of the active workloads.

A complete set of Pareto-optimal single-inlet benchmark and flow-shifting designs are generated by seeding the optimizer with random initializations ($0 \leq \varepsilon_0 \leq 1$) and random weighting coefficients ($0 \leq \alpha \leq 1$) for many repeated runs. The plot in Fig. 4 shows the two pseudo thermal resistances associated with each workload on each axis, with each point marking a design that was generated, along with selected design variable distribution maps corresponding to six selected points. The resulting data effectively forms two offset Pareto optimality fronts for the two different design approaches, where tracing along each Pareto front indicates the trade-off between the two objectives with changing weighting coefficients. All the data points are clustered near the Pareto front with some deviations caused by the use of different random initialization in each run. Nevertheless, the individual designs and Pareto front for the flow-shifting approach are universal to the lower left of the single-inlet benchmark. This indicates superior performance by the flow-shifting approach because it can always achieve a lower $R_{p,1}$ at a set $R_{p,2}$ or a lower $R_{p,2}$ at a set $R_{p,1}$. The performance difference between the two approaches is most significant within the knee region of the Pareto front ($R_{p,1} < 0.4$ K/W and $R_{p,2} < 0.4$ K/W). Outside this region, only one of the thermal resistances dominates the cost function due to a very high or very low weighting coefficient ($\alpha \to 1$ or $\alpha \to 0$) and both approaches concentrate on cooling a single workload, and therefore yield similar performance designs as would be expected. The topology optimized designs shown in Fig. 4 are highly complex regardless of the design approach used, which illustrates why design for such cases involving multiple inlets, outlets, and heated regions is not intuitive and requires formal optimization methods. Therefore, it is also not possible to easily discern the key functional difference between the two approaches just from the geometry of the designs.

One topology optimized design from each approach is investigated in further detail to understand the key differences between the designs generated by the two approaches. Designs B2 (baseline) and FS2 (flow-shifting) from Fig. 4 are chosen for further inspection because they achieve balanced thermal performance under both workloads ($R_{p,1} \approx R_{p,2}$). Details for the remaining benchmark and flow-shifting designs can be found in the Supplemental Material (Section S1). Starting with the inspection of the single-inlet benchmark design B2, Fig. 5a shows contour maps of the design variable, flow speed, flow temperature, and heat sink base temperature maps under both workloads. Because the benchmark approach uses a single inlet and fluid properties are independent of temperature, the flow speed maps are identical under both workloads. The flow enters the heat sink and is evenly distributed by the header, such that only half of the coolant is ever used to cool down each workload. The flow temperature map shows that only the coolant that is passing through the vicinity of the active workload increases in temperature, while the rest of the flow is going through a portion of the heat sink without extracting any heat, an underutilization of the available inlet heat capacity rate of the flow. The flow rates dedicated to each workload, and the consequent rise in the coolant and base temperatures, are roughly equal for this design because it was chosen from the center of the Pareto optimality curve ($\alpha \approx 0.5$). However, designs located near the ends of the curve (e.g., see B1 and B3 in Figure S1 and Figure S2 in Section S1) have features in the header regions that increase the flow resistance through one of the workloads to force it through the other direction.

An analogous compilation of design variables, flow speed, and temperature contour maps for the flow-shifting design FS2 are shown in Fig. 5.b. However, unlike the baseline, the flow-shifting heat sink uses two inlets, one dedicated to each workload. This eliminates the need for the optimizer to divide the flow to each workload from a single inlet. Hence, the resulting flow speed maps are different for the two workloads. Under either workload, the flow is directed from the inlet to its assigned heated region and thereby better utilizes the heat capacity rate available. This leads to a significantly lower temperature rise of the coolant and cooler heat sink base compared to that of the benchmark design B2 under both workloads. As discussed above in regards to the benchmark approach, flow-shifting designs near the ends of the Pareto optimality curve (e.g., see FS1 and FS3 in Figure S3 and Figure S4 in Section S1) have features in the header regions that increase the flow resistance through the workload that has a lower weight in the cost function, albeit to a lesser extent than the bench-

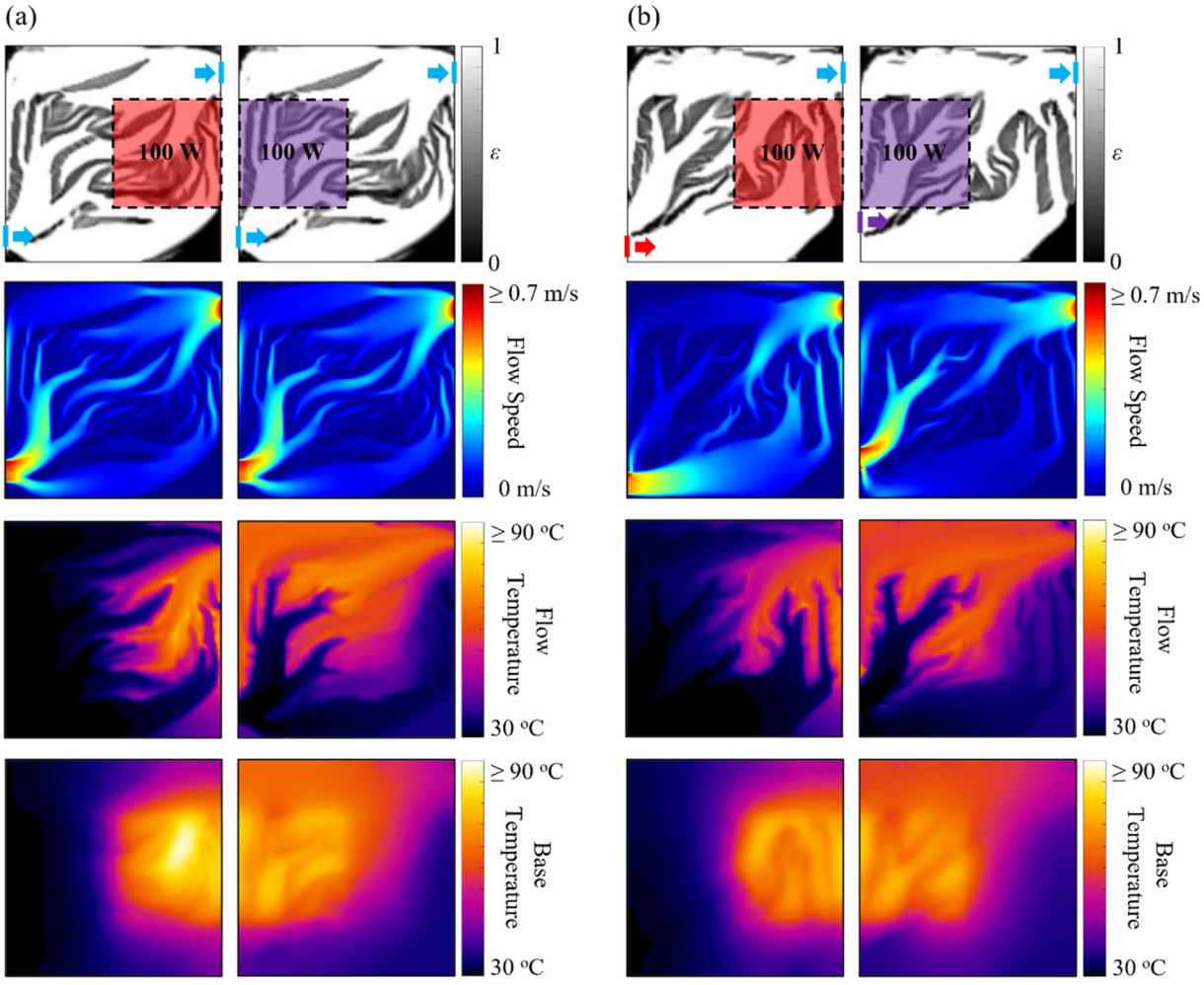

Fig. 5. Design variable, flow speed, flow temperature, and heat sink base temperature contour maps for (a) the benchmark design B2 and (b) the flow-shifting design FS2 from Fig. 4 under the two workloads.

mark. This might be perceived as counterintuitive because the flow-shifting approach uses two physically separate inlets and increasing the flow resistance through the path of a workload should ideally not alter the flow going through the other workload significantly. However, because a single physical design must be used, the two flow paths will always have some connections with flow routing through the unheated region. Heat spreading within the base allows for the fins in the unheated region to dissipate some of the heat, and therefore the optimizer does still have the ability to reduce the thermal resistance under one workload at the expense of the other.

The flow-shifting heat sink design FS2 has a 10.7% lower R_p under workload #1 compared to the benchmark design B2 and a 6.8% lower R_p under workload #2. Considering the benchmark is also a topologically optimized design, the performance advantage offered by flow shifting is quite significant. However, the performance enhancement is expected to be dependent on the exact case and operating conditions. The flow-shifting approach is beneficial under conditions where the heat capacity rate of the coolant is important to the overall performance, based on the primary mechanism of enhancement discussed above. Such conditions are more likely to exist in systems with pump curves that provide relatively low flow rates and higher pressure drop, when using high thermal conductivity heat sink materials where the conductive resistances within the heat sink base and fins are lesser, or with high thermal conductivity coolants passing through microscale features that offer low convective resistance at the fin surfaces; these qualities are all general characteristics of liquid-cooled microchannel heat sinks and their applications. In contrast, the performance enhancement provided by the flow-shifting approach will be marginalized if the conductive and convective thermal resistances are dominant over the caloric resistance.

An example case with two workloads placed in a simple configuration was used in this study such that the results could be more intuitively explained. However, the flow-shifting approach can be used with more than two workloads of arbitrarily complex spatial nonuniformity. Also, any number or combination of inlets and/or outlets can be included to create flow configuration assignments for a larger number of workloads. An additional example case with three workloads and three inlets in a relatively more complex configuration can be found in the Supplemental Material (Section S2). The performance enhancement of flow-shifting heat sinks will depend on the exact configuration of the flow and thermal boundary conditions. Although the flow-shifting approach does not strictly require topology optimization in principle, the results herein suggest such formal design methods will likely be necessary to fully leverage the performance enhancement possible. The design problem posed becomes too complicated for intuition-based design approaches to create flow-shifting heat sink geometries tailored to multiple heat maps, inlets, and outlets.

Conclusions

A flow-shifting heat sink design approach offers a way to address the challenges associated with thermal management of heterogeneous electronics having many different workloads of operation by creating specialized flow configurations for each unique heat map. These multiple flow configurations are achieved using a single, fixed heat sink geometry but with multiple different coolant inlets each assigned to a different specific workload. The heat sink geometry must be optimally designed such that each flow configuration best provides cooling of its assigned workload. Multi-objective topology optimization was used to evaluate the performance of the flow-shifting approach relative to an optimized benchmark approach which used a single inlet for all the workloads. The following key conclusions are drawn from the study:

- The topology optimized designs generated using the benchmark approach divide the available flow to each workload from the single inlet, where the division of flow rate is dictated by the weights assigned to each workload in the cost function. This results in final designs that do not fully utilize the total available heat capacity rate of the fluid under each workload. In contrast, the flow-shifting designs are able to always route a larger portion of the flow rate toward the heated regions associated with the active workload, leading to a lower temperature rise in the coolant. The flow-shifting design approach relies on this reduction in caloric thermal resistance as the primary mechanism of performance enhancement.
- In performing multi-objective optimization for addressing multiple workloads, the set of designs forms a Pareto front that reflects an inherent tradeoff between minimizing the thermal resistances of different heat maps. The optimization algorithm creates features that increase the amount of flow directed toward heated regions of the workload that is assigned a higher priority that depends on the weighting coefficient used in the cost function.
- The set of Pareto optimal designs for the flow-shifting approach has better performance than the single-inlet benchmark, always offering a lower thermal resistance for a given workload when the thermal resistance of the other workload is fixed constant. The performance enhancement achieved by the flow-shifting approach is largest within the knee region of the Pareto optimality front when the resistances of both workloads are weighted equally and $R_{p,1} \approx R_{p,2}$. However, the performance difference diminishes near the ends of the Pareto fronts(i.e., where the weighting coefficient tends as $\alpha \rightarrow 1$ or $\alpha \rightarrow 0$) because both design approaches dedicate the majority of the flow to a single workload.

Declaration of Competing Interest

The authors declare that they have no known competing financial interests or personal relationships that could have appeared to influence the work reported in this paper.

CRediT authorship contribution statement

Serdar Ozguc: Conceptualization, Methodology, Software, Investigation, Writing – original draft, Visualization. **Liang Pan:** Conceptualization, Writing – review & editing, Supervision. **Justin A. Weibel:** Conceptualization, Writing – review & editing, Supervision.

Data availability

Data will be made available on request.

Acknowledgements

Financial support for this work provided by members of the Cooling Technologies Research Center, a graduated National Science Foundation Industry/University Cooperative Research Center at Purdue University, is gratefully acknowledged.

Supplementary materials

Supplementary material associated with this article can be found, in the online version, at doi:10.1016/j.ijheatmasstransfer.2023.123933.

References

[1] S. Zeng, B. Kanargi, P.S. Lee, Experimental and numerical investigation of a mini channel forced air heat sink designed by topology optimization, Int. J. Heat Mass Transf. 121 (2018) 663–679.
[2] A.A. Koga, E.C.C. Lopes, H.F.V. Nova, C.R. de Lima, E.C.N. Silva, Development of heat sink device by using topology optimization, Int. J. Heat Mass Transf. 64 (2013) 759–772.
[3] E.M. Dede, Optimization and design of a multipass branching microchannel heat sink for electronics cooling, J. Electron. Packag. 134 (4) (2012) 041001.
[4] Y. Zhou, T. Nomura, E.M. Dede, Topology optimization of manifold microchannel heat sinks, in: 2020 19th IEEE Intersociety Conference on Thermal and Thermomechanical Phenomena in Electronic Systems, 2020, pp. 740–746.
[5] S.B. Dilgen, C.B. Dilgen, D.R. Fuhrman, O. Sigmund, B.S. Lazarov, Density based topology optimization of turbulent flow heat transfer systems, Struct. Multidiscip. Optim. 57 (2018) 1905–1918.
[6] Y. Joo, I. Lee, S.J. Kim, Topology optimization of heat sinks in natural convection considering the effect of shape-dependent heat transfer coefficient, Int. J. Heat Mass Transf. 109 (2017) 123–133.
[7] D. Martinez-Maradiaga, A. Damonte, A. Manzo, J.H.K. Haertel, K. Engelbrecht, Design and testing of topology optimized heat sinks for a tablet, Int. J. Heat Mass Transf. 142 (2019) 118429.
[8] E.M. Dede, S.N. Joshi, F. Zhou, Topology optimization, additive layer manufacturing, and experimental testing of an air-cooled heat sink, J. Mech. Des. 137 (11) (2015) 111403.
[9] B.S. Lazarov, O. Sigmund, K.E. Meyer, J. Alexandersen, Experimental validation of additively manufactured optimized shapes for passive cooling, Appl. Energy 226 (2018) 330–339.
[10] S.S. Iyer, Heterogeneous integration for performance and scaling, IEEE Trans. Component, Packag. Manuf. Technol. 6 (7) (2016) 973–982.
[11] Y. Hu, Y. Joshi, Single-phase microfluidic cooling of 2.5D-SICs for heterogeneous integration, IEEE Trans. Components Packag. Manuf. Technol. 10 (9) (2020) 1499–1506.
[12] R. Kandasamy, X.-.Q. Wang, A.S. Mujumdar, Transient cooling of electronics using phase change material (PCM)-based heat sinks, Appl. Therm. Eng. 28 (8–9) (2008) 1047–1057.
[13] G. Patankar, J.A. Weibel, S.V. Garimella, On the transient thermal response of thin vapor chamber heat spreaders: optimized design and fluid selection, Int. J. Heat Mass Transf. 148 (2020) 119106.
[14] T.A. Kingston, J.A. Weibel, S.V. Garimella, Time-resolved characterization of microchannel flow boiling during transient heating: part 1 – Dynamic response to a single heat flux pulse, Int. J. Heat Mass Transf. 154 (2020) 119643.
[15] H. Li, X. Ding, F. Meng, D. Jing, M. Xiong, Optimal design and thermal modelling for liquid-cooled heat sink based on multi-objective topology optimization: an experimental and numerical study, Int. J. Heat Mass Transf. 144 (2019) 118638.
[16] X. Dong, X. Liu, Multi-objective optimal design of microchannel cooling heat sink using topology optimization method, Numer. Heat Transf., Part A: Appl. 77 (1) (2020) 90–104.
[17] A.-.C. Iradukunda, A. Vargas, D. Huitink, D. Lohan, Transient thermal performance using phase change material integrated topology optimized heat sinks, Appl. Therm. Eng. 179 (2020) 115723.
[18] A. Banthiya, S. Ozguc, L. Pan, J.A. Weibel, Topology Optimization of an air–cooled heat sink for transient heat dissipation using a homogenization approach, in: 2022 21st IEEE Intersociety Conference on Thermal and Thermomechanical Phenomena in Electronic Systems, 2022, pp. 1–7.
[19] S. Ozguc, L. Pan, J.A. Weibel, Topology optimization of microchannel heat sinks using a homogenization approach, Int. J. Heat Mass Transf. 169 (2021) 120896.
[20] F.P. Incropera, D.P. DeWitt, T.L. Bergman, A.S. Lavine, Fundamentals of Heat and Mass Transfer, Wiley, (2011).
[21] "Material Data Sheet – AlSi10Mg-0403 powder for additive manufacturing," https://resources.renishaw.com.
[22] O. Sigmund, Morphology-based black and white filters for topology optimization, Struct. Multidiscip. Optim. 33 (2007) 401–424.